O. Holmgren, J. V. Knuuttila, T. Makkonen, K. Kokkonen, V. P. Plessky, W. Steichen, M. Solal, and M. M. Salomaa. 2005. Imaging surface-acoustic fields in a longitudinal leaky wave resonator. Applied Physics Letters, volume 86, number 2, 024101.

Imaging surface-acoustic fields in a longitudinal leaky wave resonator

O. Holmgren,[a] J. V. Knuuttila, T. Makkonen, and K. Kokkonen
Materials Physics Laboratory, Helsinki University of Technology, P.O. Box 2200 (Technical Physics), FIN-02015 HUT, Finland

V. P. Plessky
GVR Trade SA, CH-2022 Bevaix, Switzerland and Materials Physics Laboratory, Helsinki University of Technology, P.O. Box 2200 (Technical Physics), FIN-02015 HUT, Finland

W. Steichen and M. Solal
TEMEX, 06904 Sophia Antipolis, France

M. M. Salomaa
Materials Physics Laboratory, Helsinki University of Technology, P.O. Box 2200 (Technical Physics), FIN-02015 HUT, Finland

(Received 1 June 2004; accepted 10 November 2004; published online 30 December 2004)

Acoustic wave fields in a surface-acoustic-wave resonator employing the longitudinal leaky wave mode have been imaged using a scanning Michelson laser interferometer. The synchronous one-port resonator is fabricated on *YZ*-cut lithium niobate. The vibration amplitude component perpendicular to the surface has been measured at several frequencies around the fundamental-mode resonance frequency of 1.54 GHz and around the Rayleigh-wave resonance frequency of 0.82 GHz. The longitudinal beating pattern, typically observed in the resonators utilizing Rayleigh waves, is not observed in the longitudinal leaky surface acoustic-wave resonator within the measured frequency range. © *2005 American Institute of Physics*. [DOI: 10.1063/1.1849814]

Important wireless communication standards, such as Bluetooth and HiperLAN, operate in the 2–6 GHz frequency range. Leaky longitudinal surface-acoustic waves (LLSAWs)[1,2] on *YZ*-cut lithium niobate ($LiNbO_3$) manifest strong coupling, high velocity, and low losses, serving to make them a suitable propagation mode for the fabrication of low-loss high-frequency wide-band filters.[3] Due to the high velocity of the LLSAW in a periodic aluminum grating on the *YZ*-cut $LiNbO_3$ substrate ($\approx$6100 m/s), the width of the finger electrodes in the interdigital transducer (IDT) is larger than 0.25 μm even at frequencies above 5 GHz.[4] This allows for the fabrication of fundamental-mode surface-acoustic-wave (SAW) filters for frequencies as high as 5 GHz using standard optical lithography, employed in mass production of SAW devices.

At high frequencies, there are several acoustic and electrical mechanisms limiting the *Q* value of a LLSAW resonator and hence the performance of the filter constructed from these resonators. In addition to the intrinsic acoustic loss in LLSAW caused by the radiation of the shear bulk-acoustic-wave component into the substrate,[1] acoustic loss mechanisms include, e.g., viscous losses in the substrate as well as in the Al electrodes. The dominating electric loss mechanism is the resistance of the narrow finger electrodes in the IDT.

To obtain information on possible additional acoustic loss mechanisms[5] degrading the *Q* value, we have carried out laser-interferometric measurements of a synchronous one-port LLSAW test resonator. The laser interferometer setup, described in detail in Ref. 6, is an efficient tool providing direct physical information on the acoustic fields within electroacoustic devices not obtainable through measuring the electrical response. Prior to this work, LLSAW resonators have been investigated by simulations and electrical measurements. In this paper, we report direct measurements of the acoustic fields within the LLSAW resonator.

The geometrical parameters of the 1.54 GHz test resonator fabricated on *YZ*-cut $LiNbO_3$ are summarized in Table I. An interesting feature of this test device is that the substrate supports two wave forms. Therefore, in addition to the LLSAW, also Rayleigh waves are excited within the same electrode structure, designed for LLSAW operation. The two wave forms present in this resonator are illustrated in Fig. 1. Both the LLSAW and Rayleigh waves possess displacement components in the *Z* and *Y* directions (the wave propagates along the crystal *Z* axis and the surface normal is parallel to the crystal *Y* axis), but for the LLSAW, the *Z* component is dominating. The displacement component in the *X* direction is zero for both wave types. The displacement components of the Rayleigh wave decay exponentially into the bulk. However, the LLSAW is weakly coupled to the shear bulk wave, which has its displacement in the (Y,Z)-plane. This bulk wave causes propagation losses for the LLSAW through radiating energy into the substrate.

The resonance frequencies for these two wave forms are different due to the different velocities of the waves,

TABLE I. Geometrical parameters for the LLSAW test resonator. N_g and N_t are the numbers of the fingers in the short-circuited reflector grating and IDT, respectively.

Parameter	Value
Pitch (p)	2 μm
Metallization ratio (a/p)	0.60
Electrode thickness (h/λ_0)	7.9%
Acoustic aperture (W)	64 μm
No. of electrodes ($N_g/N_t/N_g$)	37/151/37

[a]Electronic mail: oholmgre@focus.hut.fi

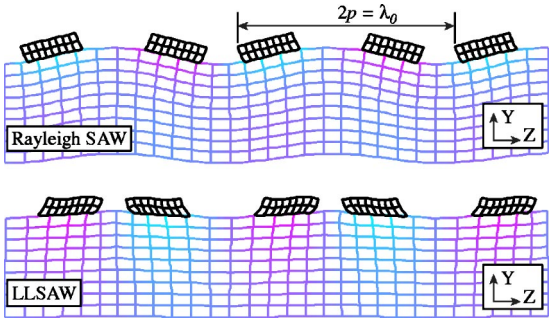

FIG. 1. (Color online). Schematic view of the Rayleigh SAW and LLSAW displacements. Both waves have displacement components in (Y,Z) plane, but for the LLSAW, the Z component is dominating. The displacements are greatly exaggerated.

~3300 m/s for the Rayleigh wave and ~6100 m/s for the LLSAW. The electrical responses, measured from a different resonator than that from which the interferometric measurements were done, are plotted in Fig. 2. Nevertheless, both resonators are diced from the same wafer and are identical to the accuracy of fabrication process. The electrical resonance for the Rayleigh wave is at 822.9 MHz and the antiresonance at 832.8 MHz. The additional peaks present in the measured admittance at 825.0 MHz, 829.5 MHz, and 836.4 MHz are due to transversal modes in the resonator, as will be discussed below. The peak at 848.8 MHz originates from the end of the stopband for the Rayleigh wave. The LLSAW

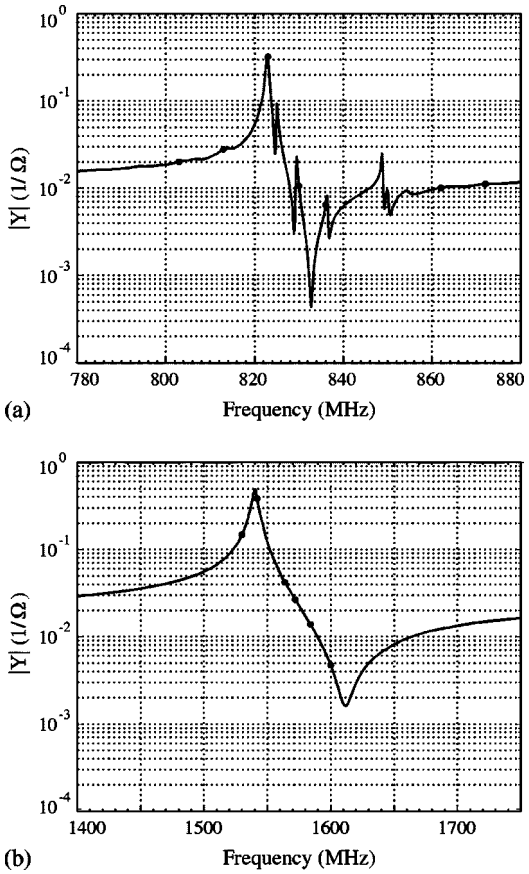

FIG. 2. Measured magnitude of the admittance as a function of frequency for (a) the Rayleigh mode and (b) the LLSAW mode. The dots indicate the frequencies for which the measured profiles are presented. The electrical response of the resonator is measured directly on the chip in 50 Ω environment.

TABLE II. Performance figures of the resonator for Rayleigh and LLSAW resonance: Resonance and antiresonance frequencies, f_r and f_{ar}, quality factors for resonance and antiresonance, Q_r and Q_{ar}, and resonance-antiresonance ratio, *r-a-r*.

Parameter	Rayleigh SAW	LLSAW
f_r (MHz)	823	1540
f_{ar} (MHz)	833	1612
Q_r	1250	310
Q_{ar}	1850	160
r-a-r (%)	1.2	4.5

response is smooth having the resonance at 1540 MHz and the antiresonance at 1612 MHz. The performance of the resonator is quantified in Table II. The temperature behavior of the LLSAW on *YZ*-cut LN has been studied by Pastureaud *et al.*,[7] who report a relatively high temperature coefficient of frequency (−105 ppm/K) for the normalized Al thickness of 8% and metallization ratio of 0.70.

The laser-interferometric measurements were carried out at 170 different frequencies around the Rayleigh and LLSAW resonance frequencies, see Table III. Each measured frequency contains 200×880 data points with a scanning step of 0.55 μm in both lateral directions. The input power fed to the resonator was +20 dBm for the LLSAW frequency range and −10 dBm for the Rayleigh frequency range. The measured profiles of the vertical vibration amplitude component at selected frequencies are presented in Figs. 3 and 4.

In the Rayleigh frequency range (Fig. 3), the scanned frequency 823 MHz is close to the Rayleigh resonance frequency. At 803 MHz and 813 MHz, a typical beating pattern in the profile along the longitudinal direction is observed. The beating pattern is due to the interference between the excited acoustic field and the propagating eigenmode. The number of antinodes increases as the frequency decreases. Above the resonance frequency at 830 MHz and 836 MHz, transversal modes are observed, which appear as stripes of high vibration amplitude along the length of the resonator. The number of antinodes in the transverse direction of the resonator increases with frequency. The origin of this transversal structure is not fully understood and its study would require simulations with a full three-dimensional (3D) model, which are presently scarcely available, only approximative models exist. At 862 MHz, the amplitude profile is even more complex. In all the scanned images in the Rayleigh frequency range, the waves propagate through the reflector gratings. This is due to the small reflection coefficient per electrode for Rayleigh waves. Since the reflectors are relatively short, they fail to confine the acoustic energy into the resonator (the resonator is designed for LLSAW).

TABLE III. Measured frequencies f. Δ is the frequency step and N is the number of frequencies in the frequency series.

Rayleigh series			LLSAW series		
f (MHz)	Δ	N	f (MHz)	Δ	N
790–818	2	15	1454–1550	4	25
820–842	1	23	1552–1616	2	33
844–898	2	28	1618–1762	4	37

Note: Additional frequencies (MHz): 791, 793, 803, 811, 813, 1563, 1565, 1567, and 1573.

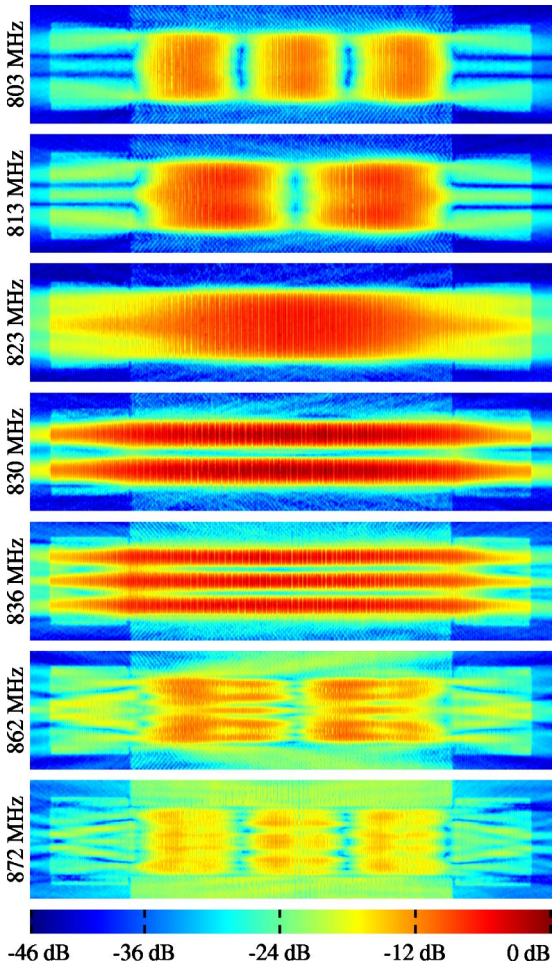

FIG. 3. (Color online). Relative amplitudes of the vertical displacement component at selected frequencies for the Rayleigh waves. Below the resonance frequency (823 MHz), the longitudinal profile possesses a typical beating pattern. Above the resonance, transversal modes are observed.

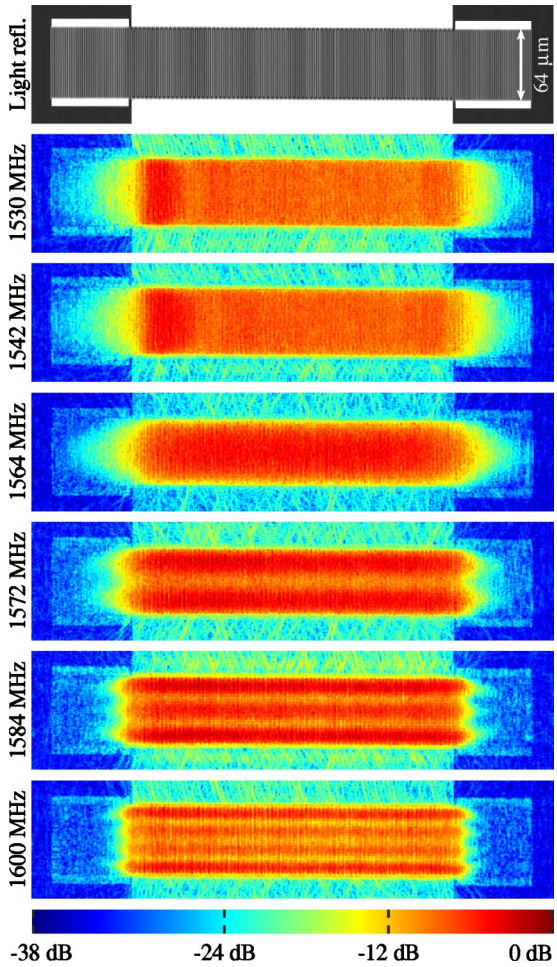

FIG. 4. (Color online). Relative amplitudes of the vertical displacement component at selected frequencies for the LLSAW. In the light reflection image, white areas represent aluminum coating and black areas, $LiNbO_3$ crystal. The beating pattern, present for Rayleigh waves in Fig. 3, is not observed here. Transversal structure appears above the resonance frequency.

In the LLSAW frequency range, the amplitude profile at 1542 MHz in Fig. 4 is selected close to the electrical resonance frequency. At the measured frequencies 1450–1540 MHz, below the lower edge of the stopband, the longitudinal beating pattern is not observed. This may be due to the high reflection coefficient per electrode for LLSAW rendering the interactions of the LLSAWs along the resonator more localized. The beating pattern typically occurs outside the stopband for Rayleigh waves and leaky SAWs,[8] and in this sense the behavior of LLSAW appears different. Above the LLSAW resonance frequency, transversal modes are observed at 1572 MHz, 1584 MHz, and 1600 MHz. However, the corresponding peaks in the electrical response, if present, are too weak to be visible. Strong attenuation of the LLSAW in the reflectors at both ends of the IDT is observed due to the high value of the reflection coefficient per electrode. The penetration depth of the LLSAW into the reflector decreases with increasing frequency in Fig. 4, as the frequency approaches the center frequency of the stopband where the reflector operates most efficiently.

In conclusion, the acoustic field profile in a LLSAW resonator on *YZ*-cut $LiNbO_3$ has been measured using the scanning laser interferometer. The beating pattern typical for Rayleigh waves is not observed for the LLSAWs within the measured frequency range. The interferometric measurements have also revealed the presence of transversal modes in the LLSAW resonator. The results are partly unexpected and stress the need for a reliable 3D simulation model for waveguide structures.

One of the authors (O.H.) thanks the Research Council of HUT for a scholarship. This research has been supported by the Academy of Finland. The authors thank their TMX colleagues for device fabrication and are grateful, in particular, to S. Chamaly for useful discussions and his interest in this work. This work has been carried out within the Eureka project E! 2442 SUMO: "New Surface-Acoustic-Wave Filter Generation for Mobile Telecommunications".

[1]V. I. Grigorievski, *Proceedings of the 2000 IEEE Ultrasonics Symposium* (IEEE, New York, 2000), p. 259.
[2]A. Isobe, M. Hikita, and K. Asai, IEEE Trans. Ultrason. Ferroelectr. Freq. Control **46**, 849 (1999).
[3]T. Makkonen, V. P. Plessky, W. Steichen, and M. M. Salomaa, Appl. Phys. Lett. **82**, 3351 (2003).
[4]T. Makkonen, V. P. Plessky, W. Steichen, S. Chamaly, C. Poirel, M. Solal, and M. M. Salomaa, Appl. Phys. Lett. **83**, 3596 (2003).
[5]J. Koskela, J. V. Knuuttila, P. T. Tikka, C. S. Hartmann, V. P. Plessky, and M. M. Salomaa, Appl. Phys. Lett. **75**, 2683 (1999).
[6]J. V. Knuuttila, P. T. Tikka, and M. M. Salomaa, Opt. Lett. **25**, 613 (2000).
[7]T. Pastureaud, S. Ballandras, and W. Steichen, *Proceedings of the 2003 IEEE Ultrasonics Symposium* (IEEE, New York, 2003), p. 200.
[8]J. Koskela, J. V. Knuuttila, T. Makkonen, V. P. Plessky, and M. M. Salomaa, *Proceedings of the 2000 IEEE Ultrasonics Symposium* (IEEE, New York, 2000), p. 209.